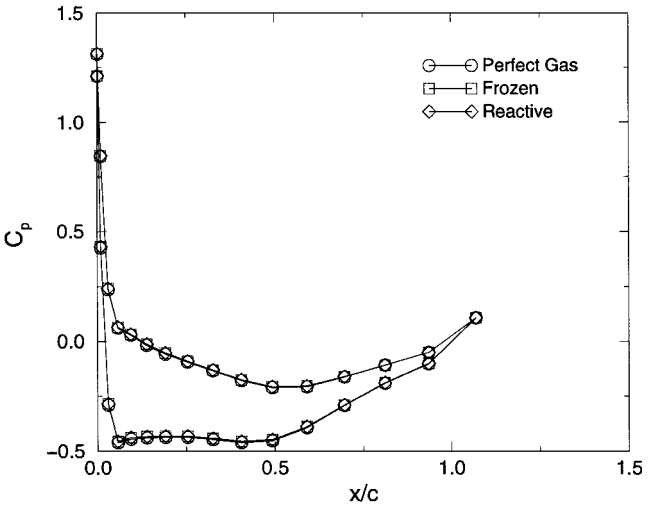

Fig. 1 Comparison of pressure coefficient predictions for M6 Onera wing at $M_\infty = 0.84$.

VI. Conclusion

The purpose of this study was to develop an eigensystem of the inviscid flux Jacobians that does not contain singularities and can be used to compute flows with finite-rate chemistry using spatially accurate methods. The eigensystem developed is valid for both flux extrapolation and dependent-variable extrapolation, higher-order-accurate extensions to the flux vector-difference scheme developed by Roe.

Acknowledgments

This work was supported in part by the National Science Foundation, which funds the Engineering Research Center for Computational Field Simulation at Mississippi State University, and by the In-House Library Independent Research Program at Carderock Division, U.S. Naval Surface Warfare Center.

References

[1]Whitfield, D. L., and Janus, J. M., "Three-Dimensional Unsteady Euler Equations Solution Using Flux Vector Splitting," AIAA Paper 84-1552, June 1984.

[2]Whitfield, D. L., Janus, J. M., and Simpson, L. B., "Implicit Finite Volume High Resolution Wave-Split Scheme for Solving the Unsteady Three-Dimensional Euler and Navier–Stokes Equations on Stationary or Dynamic Grids," Dept. of Aerospace Engineering, Rept. MSSU-EIRS-ASE-88-2, Mississippi State Univ., Mississippi State, MS, Feb. 1988.

[3]Walters, R. W., Cinnella, P., Slack, D., and Halt, D., "Characteristic-Based Algorithms for Flows in Thermochemical Nonequilibrium," *AIAA Journal*, Vol. 30, No. 5, 1992, pp. 1304–1313.

[4]Hosangadi, A., Sinha, N., and Dash, S. M., "Multi-Dimensional Simulation of ETC Gun Flowfields," U.S. Army Research Lab., Rept. ARL-CR-240, Fort Washington, PA, Aug. 1995.

[5]Liu, Y., and Vinokur, M., "Upwind Algorithms for General Thermo-Chemical Nonequilibrium Flows," AIAA Paper 89-0201, Jan. 1989.

[6]Cinnella, P., "Flux-Split Algorithms for Flows with Non-Equilibrium Chemistry and Thermodynamics," Ph.D. Dissertation, Dept. of Aerospace and Ocean Engineering, Virginia Polytechnic Inst. and State Univ., Blacksburg, VA, Dec. 1989.

[7]Busby, M. A., and Cinnella, P., "Steps Toward More Accurate and Efficient Simulations of Reactive Flows," AIAA Paper 98-2425, July 1998.

[8]Vincenti, W. G., and Kruger, C. H., Jr., *Introduction to Physical Gas Dynamics*, Krieger, Malabar, FL, 1965, Chap. 4.

[9]Hirsch, C., *Numerical Computation of Internal and External Flows*, Vol. 2, Wiley, New York, 1990, Chaps. 19, 20.

[10]Busby, M. A., "Steps Toward More Accurate and Efficient Simulations of Reactive Flows," Ph.D. Dissertation, Dept. of Aerospace Engineering, Mississippi State Univ., Mississippi State, MS, Aug. 1997.

K. Kailasanath
Associate Editor

Instantaneous Velocity Measurements Around an Oscillating Airfoil

Mark Rank*
University of Wisconsin–Platteville, Platteville, Wisconsin 53818-3099
and
B. R. Ramaprian†
Washington State University, Pullman, Washington 99164-2920

Introduction

THE study of vortex dynamics and stall associated with oscillating airfoils has been a topic of fundamental research in the aerodynamics community for many years. The details of the dynamic stall process[1] strongly depend on the airfoil geometry, the oscillation amplitude $\Delta\alpha$, the maximum incidence α_{max}, and the reduced frequency $k\ (=\pi fc/U_\infty)$, where f is the oscillation frequency, c the airfoil chord, and U_∞ the freestream velocity. McCroskey[1] identified two categories of dynamic stall, namely light stall and deep stall. Light dynamic stall, which occurs at relatively smaller values of k and moderate values of $\Delta\alpha$ and α_{max}, shares many of the features of static stall but in addition results in large hysteresis effects on aerodynamic loading. Deep dynamic stall, on the other hand, is characterized primarily by the shedding of a dynamic stall vortex (DSV). This type of stall, which occurs at larger values of k, $\Delta\alpha$, and α_{max}, leads not only to large hysteresis loops as in the light-stall case but also to very large variations in aerodynamic loading during the oscillation cycle caused by the buildup and shedding of the DSV. The present work was directed at the study of airfoil oscillation at $k = 0.05$, under which conditions the flow is expected to be characterized by light stall, in the sense just defined.

There have been several flow-visualization studies reported on the dynamic stall of oscillating airfoils. There are also extensive data on surface pressure and aerodynamic coefficients for both light and deep dynamic stall conditions. However, to the best of the authors' knowledge, there has been only one reported experiment[2] in which the instantaneous velocity field was measured on an oscillating airfoil, using the technique of particle image velocimetry (PIV). That experiment was performed at a high k value of about 0.2, at which deep stall conditions were observed. The present work represents a complementary effort to obtain data under conditions of light dynamic stall.

Description of the Experiment

This study was conducted in the large water channel facility at Washington State University. This is the same facility in which earlier dynamic stall studies have been performed in recent years. The flow facility is a 1 m wide × 0.67 m deep (3 × 2 ft) closed-loop open surface water channel. A two-dimensional NACA 0015 airfoil of 300-mm (1-ft) chord and 600-mm (2-ft) span was mounted vertically from a platform in such a way that, when rotated, the airfoil would pitch about its quarter-chord axis. The submerged end of the airfoil was fitted with an end plate to reduce end effects. This flow facility and experimental arrangement have been used extensively in the past for the study of dynamic stall of airfoils pitching at constant

Received May 2, 1998; revision received Oct. 21, 1998; accepted for publication Nov. 6, 1998.

*Database Administrator, Office of Information Technology. Member AIAA.

†Professor, School of Mechanical and Materials Engineering. Member AIAA.

angular velocity. For a more detailed description of the experimental setup, the reader is referred to Oshima and Ramaprian.[3] The airfoil was oscillated in pitch sinusoidally about its quarter-chord axis with a mean angle of incidence of 15 deg and an amplitude of 4 deg. The oscillation frequency corresponded to $k = 0.05$. The Reynolds number studied was 1.52×10^5. Pressure and lift data are available for the same airfoil geometry and oscillation conditions but at a higher Reynolds number from the experiments of Piziali.[4]

The PIV technique selected for this study is a high-density, double-exposure, direct autocorrelation method. The entire channel was seeded with 30-μm resin particles. A dual-head, solid-state Nd:YAG laser was used to illuminate the flowfield. The flowfield images were captured on a 32-exposure film roll using a Nikon F3 35-mm camera with an autoadvance attachment. The 32 photographs were evenly spaced at 0.5-deg intervals during one oscillation cycle, starting at the mean incidence of 15 deg and pitching up. To obtain a high spatial resolution, the leading-edge, midchord, and trailing-edge regions of the airfoil were photographed individually (with a slight overlap between adjacent regions) during separate experimental realizations. The results were later assembled in the analysis to obtain a composite picture of the flowfield over the entire airfoil.

The film was digitized at a resolution of 5200 pixels/in. The image was partitioned into 400 elements of 256×240 pixels, and the two-dimensional autocorrelation was estimated for each element. A peak detection and validation scheme was implemented using the peak detection technique of O'Gorman and Sanderson[5] to obtain the average particle displacement vector over each element. Further details of the PIV system and processing can be found in Ref. 6.

The spatial resolution of velocity was $0.023c$ in the streamwise x direction and $0.017c$ in the cross-stream y direction. The temporal resolution of the velocity field ranged from 2% of the oscillation period at the mean angle of attack to 5.7% of the oscillation period at the extreme ends of the oscillation cycle. The estimated experimental uncertainties are as follows: velocity, $\pm 0.05 U_\infty$; k, $\pm 2\%$; and Reynolds number, 2%.

Results and Discussion

Figure 1 shows the instantaneous streamlines for a few typical angles of incidence during the oscillation cycle. In the following discussion, we will prefix the angle of incidence with u to indicate pitch up and with d to indicate pitch down. It is seen from Fig. 1a that, just after the start of the pitch-up motion ($\alpha = $ u12 deg), a significantly thick low-velocity layer (on the order of the airfoil thickness) has formed in the aft third of the airfoil. Vorticity estimates obtained from the velocity distributions showed that vorticity levels are significant in this layer. Figures 1b and 1c show how this vortical layer further grows as the airfoil is pitched up. In Fig. 1b ($\alpha = $ u16 deg) flow recirculation begins to appear near the trailing edge. The vortical layer continues to grow and advance upstream as the angle of incidence increases until at $\alpha = $ u18 deg (Fig. 1c), this thick viscous layer extends almost up to the pitching axis of the airfoil located at the $c/4$ position. However, it is important to note that, within the resolution of the data, there is no evidence of a leading-edge vortex (LEV) even at $\alpha = $ u18.0 deg.

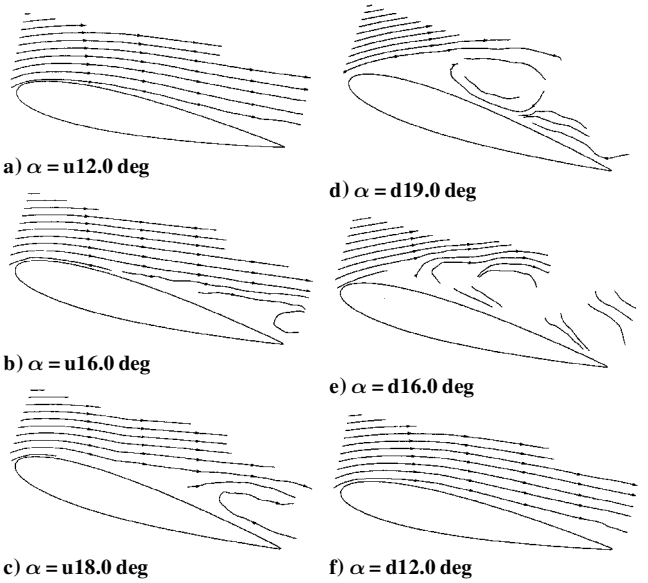

Fig. 1 Instantaneous streamlines during the oscillation cycle.

As the airfoil further decelerates toward the maximum angle of incidence, the flowfield radically changes. Figure 1d shows the flowfield at the beginning of the pitch-down cycle ($\alpha = $ d19 deg). At this point, the flowfield has separated from the airfoil surface at the leading edge, and a very thick layer of very low velocity extends over the entire surface of the airfoil. This seems to be primarily caused by the upstream advancement of the region of low and reverse velocity initially formed at the trailing edge. This flow structure, which is often described as a shear-layer vortex (SLV), is a characteristic feature of the NACA 0015 airfoil geometry. It was observed in a similar incidence range even in the uniform-pitching experiments of Oshima and Ramaprian[3] on an identical airfoil model. There is still no evidence of an LEV formation. As the airfoil continues to pitch down, this region of separated flow is convected downstream and eventually shed. This is suggested from Fig. 1e ($\alpha = $ d16 deg). During the shedding process, the flowfield associated with the SLV becomes highly disturbed. However, the velocities within the vortex were found to be very small. In fact, they were often below the resolution of the instrumentation. Hence, unlike in the case of deep stall, where a highly vortical dynamic stall vortex is shed, the vorticity shed in the present case is associated with the SLV and is quite small. Thus, the stall in the present case can be described as light. This scenario differs from that characteristic of deep dynamic stall, i.e., the initial formation of an LEV, its subsequent consolidation into a large DSV, and its eventual shedding, observed in the uniform-pitching experiments of Oshima and Ramaprian[3] and the high-frequency oscillation experiments of Raffel.[2]

The flowfield after light stall remains disturbed for most of the pitch-down part of the cycle. However, the flow pattern was found to be fairly repeatable between realizations until $\alpha \cong $ d15.0 deg, suggesting that the flowfield is reasonably periodic during this interval. As the pitch down continues beyond d15.0 deg, the flow begins to reattach. This reattachment process was found to vary from one realization to another, suggesting that the process is nonperiodic. Such a lack of periodicity was also observed in the experiments of Raffel.[2] In the present experiments the periodicity is eventually recovered when the reattachment process is complete. This occurs at $\alpha \cong $ d12 deg, as seen from Fig. 1f. The flow remains attached for the remainder of the pitch-down cycle, after which a new oscillation cycle starts.

Another important feature of the flow over an oscillating airfoil is the phenomenon of hysteresis, i.e., a lack of symmetry between the pitch-up and pitch-down parts of the cycle. This leads to a hysteresis loop in the lift-vs-incidence curve that has been observed in all of the experiments on oscillating airfoils. This can also be seen from Figs. 2a–2d, which show the variation of the thickness of the vortical layer at four different chordwise locations during the oscillation cycle. For this purpose, the thickness of the vortical layer at any longitudinal station on the airfoil was defined (arbitrarily) as the thickness where the vorticity has dropped to 10% of the maximum vorticity at that station. Filled symbols in Figs. 2a–2d indicate pitch-up motion, and open symbols indicate pitch-down motion.

At the $x/c = 0.20$ station (Fig. 2a), the vortical layer remains very thin for most of the pitch-up portion of the oscillation cycle. During the pitch-down part of the cycle, the vortical layer thickness increases to 10% of the chord and then returns to the initial thickness at d13.0 deg, resulting in the characteristic thumb-shaped hysteresis loop. There is more activity in the growth of the vortical layer at $x/c = 0.36$ (Fig. 2b). At this station, the vortical layer starts out slightly thicker, increases gradually to 8% of the chord at u18.deg,

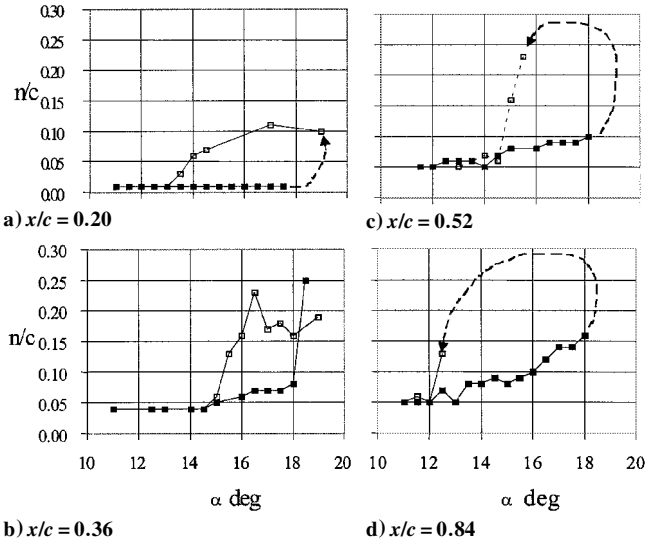

Fig. 2 Variation of the vortical layer thickness during the oscillation cycle: Filled symbols denote pitch up, and open symbols denote pitch down.

and then jumps to 25% of the chord at u18.5 deg. This corresponds to the arrival of the reversed-flow region (SLV) in its upstream movement along the airfoil surface. The results at $x/c = 0.52$ and 0.84 (Figs. 2c and 2d) show a similar trend, differing only in the timing of the events. In each case, the initial viscous layer, which is already quite thick, further thickens as the incidence increases to u18.0 deg. At this point it is no longer possible to define a vortical layer thickness because the boundary of the vortical layer has moved outside the visualization field. In each case, during the downward pitching phase of the oscillation, the flow recovers, completing the hysteresis loop, even though only a part of the thumb curve lies within the field of vision.

Conclusions

The present investigation of the oscillating airfoil showed that, under the operating conditions studied, the airfoil undergoes light dynamic stall. This stall process is characterized by the formation, growth, and upstream movement of a vortical layer in the aft region of the airfoil, leading to large-scale flow separation and eventual shedding of a weak vortex, the so-called SLV. No LEV formation or the scenario associated with deep stall was observed during the pitch-up motion. The initiation of the stall process from the trailing edge is believed to be characteristic of the NACA 0015 airfoil section tested. The experiments also indicated strong hysteresis effects in the flow evolution. The present velocity data are consistent with pressure and lift measurements on oscillating NACA 0015 airfoils reported in the literature.

References

[1]McCroskey, W. J., "Unsteady Airfoils," *Annual Review of Fluid Mechanics*, Vol. 14, 1982, pp. 285–311.

[2]Raffel, M., "PIV-Messungen instationärer Geschwindigkeitfelder an einem schwingenden Rotorprofil," DLR, Rept. DLR-FB-93-50, Göttingen, Germany, Oct. 1993.

[3]Oshima, H., and Ramaprian, B. R., "Velocity Measurements over a Pitching Airfoil," *AIAA Journal*, Vol. 35, No. 1, 1997, pp. 119–126.

[4]Piziali, R. A., "2-D and 3-D Oscillating Wing Aerodynamics for a Range of Angles of Attack Including Stall," NASA TM-4632, Sept. 1994.

[5]O'Gorman, L., and Sanderson, A., "The Converging Squares Algorithm: An Efficient Method for Locating Peaks in Multidimensions," *IEEE Transactions on Pattern Analysis and Machine Intelligence*, Vol. 8, No. 3, 1984, pp. 280–288.

[6]Rank, M., "PIV Study of the Two-Dimensional Flow Field Around an Oscillating Airfoil," M.S. Thesis, School of Mechanical and Materials Engineering, Washington State Univ., Pullman, WA, Dec. 1997.

A. Plotkin
Associate Editor

Effect of Thickness on Large-Deflection Behavior of Shells

Reaz A. Chaudhuri* and Raymond L. Hsia†
University of Utah, Salt Lake City, Utah 84112

Introduction

INVESTIGATIONS pertaining to the effect of transverse shear/normal deformation on the large-deflection behavior of moderately thick shells appear to be absent in the literature, although such an effect has been thoroughly investigated in the small-deflection regime (see, e.g., Ref. 1). The primary objective of the present research is to investigate thoroughly the combined effects of geometric nonlinearity and transverse shear/normal deformation on the large elastic deformation behavior of moderately thick shells and panels of finite dimensions. Second, the question of what the Kirchhoff hypothesis means in the nonlinear regime still remains unsettled. Obviously, it cannot be the same as its linear counterpart. This triggered our interest in developing the fully nonlinear kinematic formulation for moderately thick shells as opposed to its von Kármán counterpart.

The present analysis accounts for all of the nonlinear terms in the kinematic relations and utilizes the total Lagrangian formulations in incremental equilibrium equations. A nonlinear, moderately thick shell, finite element methodology is developed to obtain the discretized system equations. The element is capable of accurately modeling the curved geometry of a shell, taking advantage of a tensorial formulation that uses the surface-parallel curvilinear coordinates of non-Euclidean geometry. The present nonlinear finite element solution methodology is based on a quasi-three-dimensional hypothesis known as linear displacement distribution through thickness (LDT) theory.[2] A curvilinear-side, 24-node element with 12 nodes on each of the top and bottom surfaces of a shell is implemented to model the quasi-three-dimensional interlaminar deformation behavior represented by the LDT. The Broyden–Fletcher–Goldfarb–Shanno (BFGS) iterative scheme[3] is used to solve the resulting nonlinear equations. A thin/shallow clamped cylindrical panel is investigated to test the convergence of the present element and to compare the present solution with the available numerical results. The convergence rate of the present serendipity-type cubic element is compared with that of its quadratic counterpart. Additionally, numerical results for shallow clamped cylindrical panels are presented to provide new insights into certain interesting deformation behaviors of thick and thin homogeneous isotropic cylindrical panels in the advanced nonlinear regimes. The relative (to linear) nonlinear membrane-to-shear effect, defined as the ratio of normalized deflections computed using the nonlinear and linear analyses, studied here for the first time, sheds new light on the relative roles of transverse shear/normal deformation and surface parallel membrane effects in thin to thick shell regimes.

Isoparametric Finite Element Discretization

The convected coordinates of a generic point (x^1, x^2, z) in an element with 12 nodal points on each of the top and bottom surfaces are, in terms of the natural coordinates r, s given by

$$x^j(r,s,z) = \left(1 - \frac{z}{h}\right)\sum_{k=1}^{12}\psi_k(r,s)_b x_k^j + \frac{z}{h}\sum_{k=1}^{12}\psi_k(r,s)_t x_k^j \quad \text{for} \quad j = 1,2 \quad (1a)$$

Received April 3, 1997; revision received Sept. 18, 1998; accepted for publication Oct. 6, 1998.

*Associate Professor, Department of Materials Science and Engineering. E-mail: R.Chaudhuri@m.cc.utah.edu.

†Graduate Research Assistant, Department of Civil Engineering; currently Assistant Squad Leader, Structures Division, Utah Department of Transportation, Salt Lake City, UT 84119.